An unsupervised context-free forecasting method for structural health monitoring by generative adversarial networks with progressive growing and self-attention

Shuai Gao[1], Zhengbo Zou[2], Zhenwei Zhou[3] (ID), Chunfeng Wan[1] (ID), Liyu Xie[4] (ID) and Songtao Xue[4,5]

Abstract

Ensuring the robust operation of bridges demands swift and precise forecasting of structural performance within the health monitoring system. However, challenges arise in the realm of long-time series forecasting context-free data. These challenges encompass scenarios where there is a lack of reference data pre- and postforecasting, instances of missing data before forecasting (near-forecasting), or predictions of the distant future (far-forecasting). Addressing these issues, a current imperative is the development of a framework adept at efficiently and directly forecasting context-free long-time series data. This article introduces a framework, the convolutional generative adversarial network with progressive growing and self-attention (PSA-CGAN) mechanisms, tailored for forecasting context-free data. The approach employs generative adversarial networks in tasks related to long-time series. Additionally, progressive growing and self-attention mechanisms are harnessed to capture both long- and short-term features in the time series, notably enhancing the efficiency and accuracy of the forecasting method. The proposed method undergoes validation through application to two distinct bridge cases, confirming its generality and real-time forecasting prowess. On two bridges, PSA-CGAN can effectively predict acceleration data in various context-free scenarios and is capable of forecasting progressively changing damage data. It provides a valuable reference for predicting damage data. Additionally, the results indicate that PSA-CGAN is a promising and practical solution for the prediction of context-free data. It represents an efficient and rapid tool for damage prediction.

Keywords

Structural health monitoring, context-free forecasting, generative adversarial networks, progressive growing, bridge

Introduction

To ensure the stability and safety of large-scale infrastructure projects such as bridges, skyscrapers, and dams during their operational lifetimes, structural health monitoring systems have been widely implemented.[1–7] Within the context of structural health monitoring systems for bridge structures, the rapid and accurate prediction of structural performance to ensure the healthy operation of bridges has become a top priority. However, there are challenges in the field of long-term time series prediction without contextual information, such as predicting without reference data, dealing with data gaps prior to prediction (normal forecasting), or forecasting far into the future (long-

[1]Southeast University, Key Laboratory of Concrete and Prestressed Concrete Structure of Ministry of Education, Nanjing, China
[2]Department of Civil Engineering, University of British Columbia, Vancouver, BC, Canada
[3]School of Civil Engineering and Architecture, East China Jiao Tong University, Nanchang, China
[4]Department of Disaster Mitigation for Structures, Tongji University, Shanghai, China
[5]Department of Architecture, Tohoku Institute of Technology, Sendai, Miyagi, Japan

Corresponding author:
Chunfeng Wan, Southeast University, Key Laboratory of Concrete and Prestressed Concrete Structure of Ministry of Education, Sipailou 2#, Nanjing 210096, China.
Email: wan@seu.edu.cn

term forecasting). These challenges have not yet received sufficient research attention. Current research methods typically employ a two-step approach, where missing data are first filled using imputation methods, followed by the application of prediction methods to forecast future data. This dual-method approach results in lower efficiency. Furthermore, many prediction methods cannot be directly applied to the task of long-term time series prediction without context, and most methods are designed for short-term time series prediction tasks. Therefore, one of the current challenges is to design a framework that can efficiently and directly predict long-term time series data without contextual information.

In the realm of data prediction, prevalent methods can be broadly categorized into two types: those grounded in statistical approaches and those rooted in machine learning methods. Statistical time series forecasting models are widely recognized for estimating structural responses. Specifically, parametric and non-parametric methods are two main types for statistical time series modeling, based on discretized excitation and response random vibration data records. Non-parametric methods are easily trainable and highly efficient, albeit at the expense of forecasting performance. On the other hand, parametric methods offer superior performance but are applicable only to a limited dataset.[8] Owing to their predominantly brief application in time series and their inability to meet accuracy and efficiency requirements, statistical learning methods are rarely employed.

In recent decades, machine learning has emerged as a promising solution to address the challenges mentioned earlier. Han et al.[9] provided a summary of forecasting methods for predicting and isolating temperature-induced components of overall responses, including regression analysis (RA), support vector machine (SVM), artificial neural network (ANN), principal component analysis (PCA), empirical mode decomposition (EMD), and more. While RA methods are easily applicable for forecasting structural responses with simple and explicit formulas, their performance suffers in the presence of nonlinear relationships between temperature and responses. Notably, SVM and ANN can address these issues, albeit at the expense of clear and explicit modeling formulas. PCA excels in analyzing current responses but struggles to separate and predict future responses under complex nonlinear environmental effects. EMD is effective in analyzing dynamic response data at specific sampling frequencies under the influence of various environmental factors (e.g., temperature, wind speed), yet it faces challenges in analyzing static data with low-frequency sampling. In addition, Kang et al.[10] introduced a response prediction method based on long-term air temperature, combining the Jaya optimizer, salp swarm algorithms, and SVM algorithms to forecast monitoring data for a concrete gravity dam. Importantly, this method doesn't pose a significant computational burden, especially when the number of training samples is not very large.

Bayesian methods stand out as crucial in machine learning forecasting. Wan and Ni[11,12] introduced structural response forecasting frameworks employing Bayesian modeling methods. However, the traditional Bayesian forecasting approach faces challenges in reliably predicting missing data in certain cases when using different covariance functions. Wang and Ni[13] proposed a Bayesian dynamic linear model (BDLM) capable of forecasting both stationary and nonstationary time series data. It delineates the time-dependent structural strain response by invoking various hidden components, including overall trend, seasonal (cyclical), and regressive components. In a related work, Wang and Ni[14] presented a BDLM framework for forecasting structural responses in the context of typhoon-induced nonstationarity, large data fluctuations, and strong randomness in existing in-service bridges. Notably, the BDLM framework yields robust results by leveraging monitoring data both before and after the missing segments. Latterly, Ren[15] introduced Bayesian and Tensor analysis to forecast random missing strain and temperature in concrete bridges. This approach constructs one-dimensional data as second- or third-order tensors, mining reliable underlying characteristics rather than directly utilizing the original incomplete data. Green and Jaspan[16] employed a Bayesian approach with uncertainty quantification (UQ) techniques for anomaly detection and forecasting inclinometer data. Yi et al.[17] proposed a Bayesian robust tensor learning model to reconstruct monitoring data tensors by extracting potential spatiotemporal data features. Additionally, Lai et al.[18] utilized partially observable Markov decision processes and Bayesian forecasting to predict the life-cycle condition, including cycling impacts and estimating deterioration rates, under stochastic environments using actual long-term monitoring data.

Wei et al.[19] enhanced dam displacement time series forecasting by employing a combination of backpropagation neural network and the autoregressive integrated moving average (ARIMA) model. This approach effectively addresses both high-frequency and low-frequency signals, leading to improved forecasting precision and convergence speed. Yang et al.[20] introduced singular spectrum analysis (SSA) to predict the long-term trend and short-term fluctuation of strains. Comparative results demonstrate the superiority of SSA over the ARIMA model. Subsequently, Qu et al.[21] proposed fitted models, specifically the seasonal

SARIMA model, for predicting future development trends based on current and previous monitoring data. In a related study, Zhang et al.[22] utilized two autoregressive (AR) based matrix factorization (MF) methods to forecast spatiotemporal structural monitoring time series. To enhance efficiency in computing nonlinear structural dynamics responses, an innovative graph-based temporal regularizer was incorporated with standard MF. Simultaneously, the AR-based matrix was introduced to forecast spatiotemporal structural information. Later, Wang and Zhang[23] suggested a combined approach involving the AR model and MF method with a graph-based temporal regularizer for data imputation prediction. This method effectively captures cyclic characteristics and random variability.

Wang and Ni[24] leveraged the heteroskedasticity characteristics of Variational Heteroscedastic Gaussian Process, employing a fusion of variational approximation and heteroscedastic Gaussian process. This innovative approach was applied to forecast strain field data in structural health monitoring (SHM) during typhoon events, resulting in heightened forecasting precision and reduced uncertainty.

The generative adversarial network (GAN) has become a focal point in research due to its outstanding generative capabilities and has been widely applied in fields such as image and sound synthesis.[25–27] Its application scope has gradually expanded into the field of time series, with the current network framework primarily utilizing recurrent networks to perform time series generation tasks. However, as the length of time series increases, its application effectiveness diminishes. Yoon et al.[28] use GANs for the reconstruction of missing data, while Jiang, et al.[29–32] enhance GANs by applying hint mechanisms and data augmentation to improve the accuracy of generated data. Additionally, Lei et al.[33] demonstrate that GANs generate signals by learning features at different frequencies. Fan et al.[34,35] propose improvements to the SegGan architecture, incorporating skip connections and dense blocks for reconstructing short-term acceleration data in numerical simulations and steel frameworks. However, there are still some shortcomings in the application of time series, especially when dealing with long-time series. For example, modeling long-term dependencies and extending recurrent networks to long-time series face significant challenges, restricting the application of time series GANs to long-time series lengths. To achieve longer and more realistically synthesized time series, one approach is to adopt a convolutional network framework. However, traditional convolutional modules primarily capture short-term dependencies in the data. Therefore, current research lacks in enhancing

data accuracy, especially in extracting short-range and long-range information in long-time series data.

This article introduces a convolutional generative adversarial network with progressive growing and self-attention (PSA-CGAN) for context-free data prediction. This method applies GANs to tasks involving long-time series data. Furthermore, the article incorporates two crucial mechanisms, progressive growing and self-attention, to capture both long-term and short-term features within long-time series data, significantly enhancing the efficiency and accuracy of the prediction method. Additionally, the method is applied to two different bridge cases to validate its versatility and real-time prediction capability.

The structure of the article is as follows: section "The proposed unsupervised damage forecasting" provides a detailed overview of the framework structure and theoretical background of this method; section "Application case study I: Tongling bridge" presents the results of applying this method to the undamaged scenario of the Tongling dual-purpose railway and highway bridge over the Yangtze River; section "Application case study II: Z24 bridge" demonstrates the results of applying this method to the damage scenario of the Z24 bridge (as a benchmark model); section "Conclusion" primarily discusses the main conclusions of this paper.

The proposed unsupervised damage forecasting

This section demonstrates the proposed unsupervised framework for forecasting structural damage and conditions in bridge structures equipped with SHM systems. This approach is principally utilized for far-forecasting the context-free acceleration sensors in SHM systems.

Problem demonstration

When it comes to the daily monitoring system for the health of bridge structures, accurately predicting data from critical node sensors becomes paramount. This aids in better analyzing and monitoring the state of the structures. However, a challenge is encountered in data prediction tasks, which is making predictions without contextual information. This can significantly impact the accuracy of the data and the credibility of the analysis results. As shown in Figure 1, predictions without context can typically be categorized into two scenarios: long-term forecasting (far-forecasting) and short-term forecasting (near-forecasting).

In the past, researchers often followed a two-step approach, initially filling in missing data and then
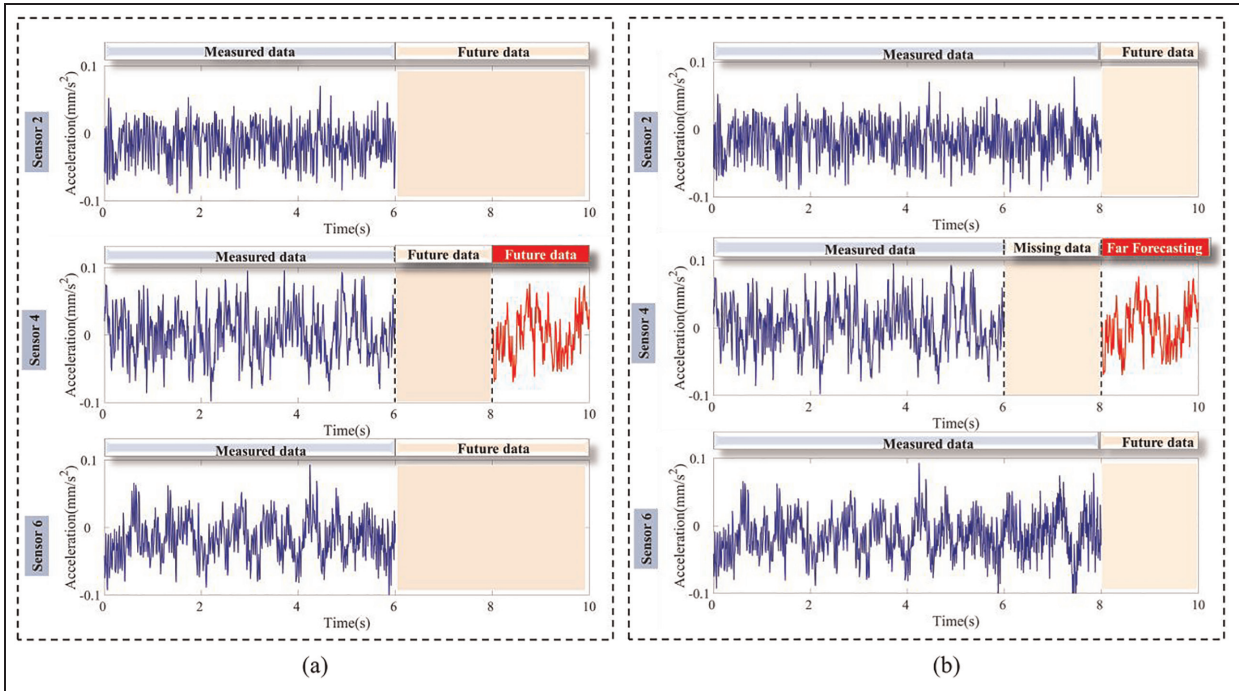
Figure 1. The data forecast with context-free: (a) near-forecasting and (b) far-forecasting.
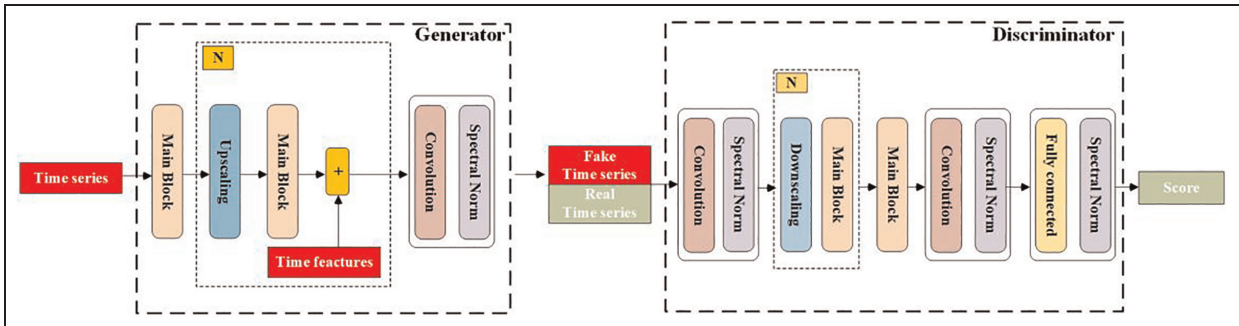

Figure 2. Architecture of convolutional generative adversarial network with progressive growing and self-attention.

applying prediction methods to forecast the data. Furthermore, many researchers focused on short-series data, which do not meet the widespread demand for long-time series data today. Therefore, finding an appropriate, efficient, and direct prediction method has become especially important. This article is based on a data-driven approach and aims to directly address the challenge of predicting long-time series data in situations where contextual information is absent.

Training of the PSA-CGAN

This article presents "PSA-CGAN," a context-free prediction method based on a convolutional GAN that integrates progressive growing and self-attention functionalities. The network architecture resembles

common GAN structures, comprising a generator and a discriminator, as depicted in Figure 2. The generator and discriminator structures are mirror-like, each consisting of N main blocks with convolution and spectral normalization modules. Notably, they differ significantly in key aspects. To extract subtle features effectively, the generator utilizes a combination of convolution and upscaling techniques. In contrast, the discriminator employs a mix of convolution and downscaling methods to filter out irrelevant small features while retaining crucial information.

In the context of GAN applications, recurrent neural networks are often applied to time series data, focusing on short-term series. To overcome the limitation in handling long-time series, convolutional neural networks are introduced to capture relevant features
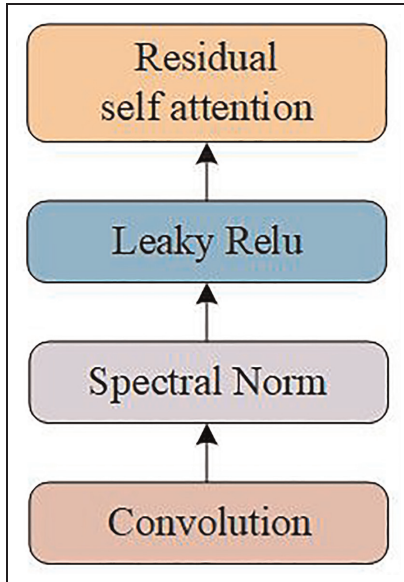
Figure 3. The structure of main block.

over extended periods. However, traditional convolutional modules primarily capture short-term dependencies. To address this, we enhance PSA-CGAN's ability to capture remote dependencies by introducing the self-attention mechanism, modeling distant dependencies within the convolutional feature maps.

Furthermore, the progressive growing module can better capture features in long-time series. During training, this module initially extracts time features over extensive intervals and subsequently captures detailed time features, providing a comprehensive understanding of temporal information in the time series data. Additionally, PSA-CGAN incorporates spectral normalization and progressive growing modules to improve training stability.

Main function

As shown in Figure 3, the main function is a crucial component of both the generator and the discriminator. It consists mainly of three parts: convolution, self-attention, and spectral normalization. The activation function used is LeakyReLU, as expressed in Equation (1). The self-attention part involves a parameter named "gamma (γ)," which starts from zero to encourage learning of detailed time features and gradually increases as the network learns broader time features. Additionally, both the generator and the discriminator benefit from using spectral normalization layers. In the discriminator, spectral normalization contributes to stable training by constraining the Lipschitz constant of the discriminator to be within the bound of 1. In the generator, spectral normalization stabilizes training

and prevents the unstable increase in gradient magnitude. In addition, convolutional network architecture, compared to common recurrent network architectures, not only saves memory but also proves to be more efficient.

$$M(x_i) : x_i \rightarrow \gamma \text{SA}(\text{LR}(\text{SN}(\text{CONV}(x_i)))) + \text{LR}(\text{SN}(\text{CONV}(x_i))) \quad (1)$$

where SA is referenced as self-attention; LR represents LeakyReLU activation; SN denotes Spectral normalization, CONV denotes convolution; x_i denotes time series; λ is learnable.

Progressive growing architecture

PSA-CGAN can be extended to long-time series because it adopts a progressive growing architecture, starting with modeling coarse-grained time series features and gradually iterating toward finer-grained details during training. This architecture can generate longer series by increasing the number of blocks. To ensure stability when adding new blocks and avoid instability caused by the random initialization of new, untrained parameters, progressive growth techniques are utilized to smoothly incorporate new blocks.

The primary contribution of progressive growing is an improvement in GAN training methods. We begin modeling with coarse-grained time series features and then progressively add finer-grained time series features, as illustrated in Figure 4. This incremental approach allows training to initially capture large-scale structural aspects of the data distribution and then gradually shift attention toward increasingly finer-scale details, without the need to simultaneously learn all scales.

In this article, generator and discriminator networks that mirror each other are employed, growing synchronously throughout the training process. All existing layers in both networks are trainable. When adding new layers, the layers are smoothly used to prevent sudden disruptions to already well-trained fine-grained time series features.

Progressive training offers several benefits. In the early stages, generating coarse-grained time series features is more stable, as there is less class-specific information and simpler patterns to capture. By gradually increasing the granularity of time series features, we incrementally tackle increasingly complex challenges, without the immediate need to solve the final goal of mapping from latent vectors to real data, among other objectives.

Another advantage is reduced training time. For progressive growing GANs, the majority of iterations are completed with coarse-grained time series features.
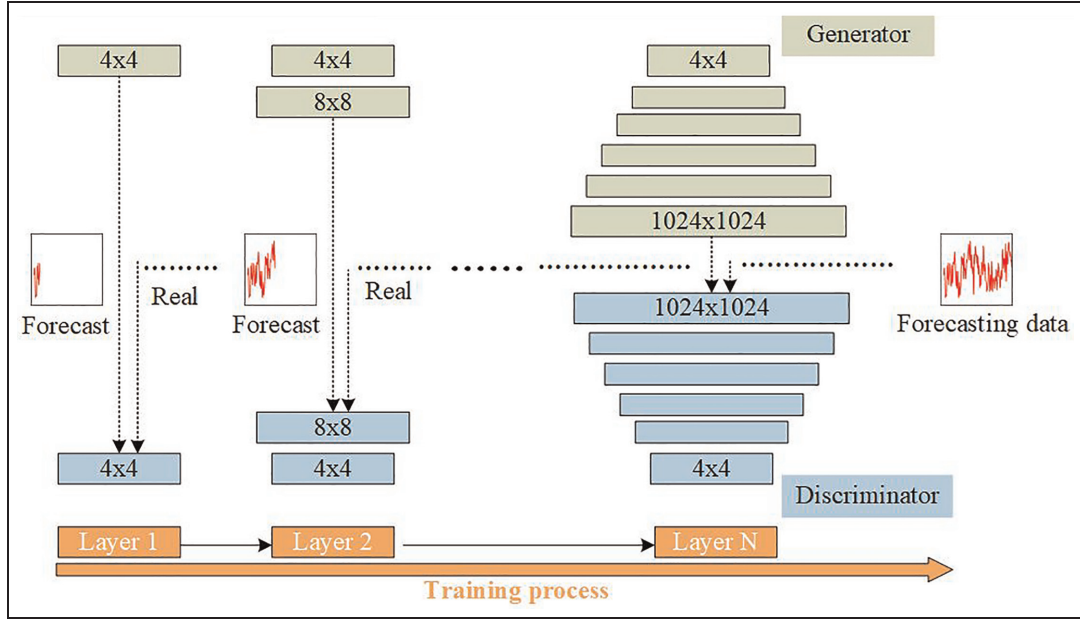
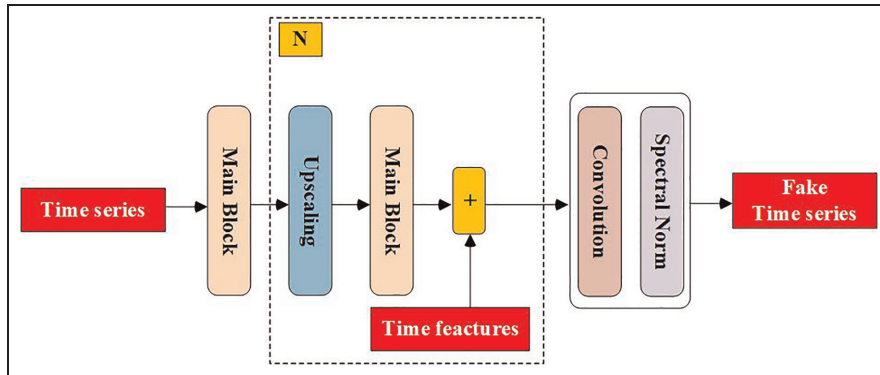**Figure 4.** The training process of progressive growing architecture.

Figure 5. The structure of generator.

This typically results in shorter training times while achieving comparable result quality.

Structure of generator

The generator, as an indispensable component of PSA-CGAN, receives inputs from time series. Its output consists of the generated data, which also serve as input for the discriminator. Furthermore, the discriminator can be divided into three hierarchical layers, as depicted in Figure 5.

First, the first layer primarily comprises main blocks, with computations as shown in Equation (2). To accommodate long-time series applications, the second layer adopts a progressive growing architecture. In second layer, it mainly consists of N upscaling operations and main blocks, with computations detailed in Equation (3). To better capture minute features, upscaling employs the method of maximum interpolation. The third layer mainly consists of modules composed of convolution and spectral normalization, with calculations as shown in Equation (4).

First layer:

$$G_1 : X_0 \rightarrow X_1 = M(X_0) \tag{2}$$

Secondary layer to penult layer:

$$G_i : X_{i-1} \rightarrow X_i = M(UP(X_{i-1})) \tag{3}$$

Last layer:

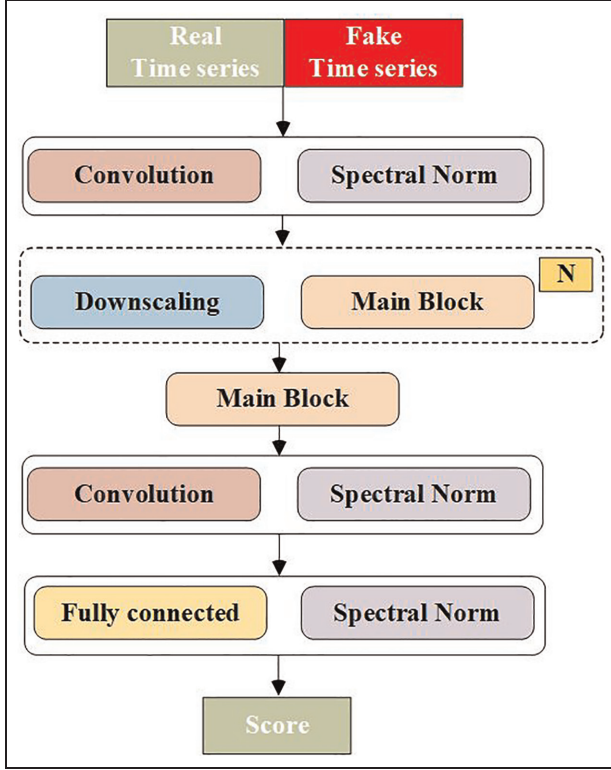$$G_{i+1} : X_i \rightarrow X_{i+1} = SN(LR(CONV(X_i))) \tag{4}$$

Figure 6. The structure of discriminator.

where M represents Main function; LR represents LeakyReLU activation; UP denotes upscaling operations, CONV denotes convolution; SN denotes Spectral Normalized; X_i denotes time series in generator.

Structure of discriminator

As a crucial component of PSA-CGAN, the discriminator's structure divides its input into two parts: one corresponds to the length of the data generated by the generator (fake time series), while the other corresponds to the length of real data (real time series). Its output is a score used to assess the generated data, to adjust this score appropriately to make it as close to real data as possible. Additionally, the discriminator can be categorized into three levels, with its structure depicted in Figure 6.

First, the first layer primarily consists of convolution and spectral normalization, calculated as shown in Equation (5). To accommodate long-time series applications, the second layer employs a progressive growing architecture. In second layer, it mainly comprises N downsampling operations and main blocks, with calculations detailed in Equation (6). To filter out irrelevant small features while retaining critical information, downscaling employs the average pooling method.

The third layer primarily consists of modules composed of main blocks, convolution, and spectral normalization, complemented by fully connected layers and modules utilizing spectral normalization, with calculations as depicted in Equation (7). In the end, the input series is mapped into a score by using a fully connected layer and the spectral normalization.
First layer:

$$D_{i+1} : X_{i+1} \to Y_i = \mathrm{SN}(\mathrm{LR}(\mathrm{CONV}(X_{i+1}))) \quad (5)$$

Secondary layer:

$$D_i : Y_i \to Y_{i-1} = \mathrm{DOWN}(M(Y_i)) \quad (6)$$

The last module:

$$D_1 : Y_1 \to Y_0 = \mathrm{SN}(\mathrm{FC}(\mathrm{LR}(\mathrm{CONV}(M(Y_i))))) \quad (7)$$

where SN denotes spectral normalized; LR represents LeakyReLU activation; CONV denotes convolution; FC denotes fully connected layer; M represents main function; Y_i denotes time series in discriminator.

Loss function

In traditional GANs, the discriminator is treated as a classifier and uses the cross-entropy function as the loss function. This method is prone to issues such as gradient vanishing and mode collapse. This article addresses these issues by using least squares loss instead of cross-entropy loss, thereby improving data generation quality and stabilizing the training process in traditional GANs.

In traditional GANs, when the generator produces fake data that are classified as real by the discriminator, updating the generator's parameters may lead to gradient vanishing. Even though these fake data points are still far from real data, the generator stops optimizing them because the cross-entropy loss is already very small. This means the quality of the generated data is not high. When using least squares loss, the discriminator pulls the fake data toward the decision boundary, which passes through real samples, making the generated data closer to the real data. The least squares loss function penalizes data that are far from the decision boundary, pushing it toward the boundary and thus avoiding the gradient vanishing problem.

The learning process of traditional GANs is unstable, especially due to the gradient vanishing problem, which makes it difficult to update the generator and leads to training difficulties. Cross-entropy loss easily reaches saturation (i.e., zero gradient), further increasing training difficulty. The least squares loss penalizes generated samples based on their distance from the boundary, avoiding the gradient vanishing

problem and making the training process more stable. Unlike cross-entropy loss, least squares loss only saturates at one point, thus providing a continuous gradient signal during training.

In addition, the introduction of progressive growing technology enhances training stability by smoothly increasing the training layers. The use of spectral normalization layers benefits both the generator and the discriminator. In the discriminator, spectral normalization stabilizes the training process by constraining the Lipschitz constant to be within 1. In the generator, spectral normalization also stabilizes training and effectively prevents the escalation of gradient magnitudes.

Empirical evidence shows that the combination of least squares method, progressive growing technology, and spectral normalization can effectively stabilize the training process of PSA-CGAN.

It is well-known that the suitable loss function decides the stability of training process in GAN. In this article, the application of loss function effectively mitigates the model collapse and gradient vanishing. The loss can be calculated as the absolute sum of two components: one measures the mean difference between forecasted time series and raw time series, while the other quantifies the disparity in standard deviation between forecasted and raw time series:

$$\text{Loss} = |F_{\text{Mean}} - R_{\text{Mean}}| + |F_{\text{Std}} - R_{\text{Std}}| \quad (8)$$

where F_{Mean} denotes the mean of forecasting time series; R_{Mean} denotes the mean of raw time series; F_{Std} denotes the standard deviation of forecasting time series; R_{Std} the standard deviation of raw time series.

Application case study I: Tongling bridge

To evaluate the predictive prowess of the PSA-CGAN framework, a practical study is conducted on the acceleration of a dual-purpose road and railway bridge. Utilizing the PSA-CGAN framework, the acceleration for 14 key and undamaged sensors on the bridge under various context-free scenarios are successfully forecasted. The forecasting framework is applied in pytorch, and the configurations of the computational platform are two Intel Xeon(R) E5-2696 v4 CPUs, a 256 GB memory, and an NVIDIA TITAN X (Pascal) GPU for boosting algorithm application. The hyperparameters of the models are presented in Table 1. Furthermore, the identical configuration is employed across all other scenarios discussed in this article. The implemented process of the data forecasting method will be discussed in detail below.

Table 1. Hyperparameters of model.

Hyperparameters	Value
N (Number of blocks)	2
Batch size	121
Epoch	50
Optimizer	Adam
Learning rate (generator)	0.0005
Learning rate (discriminator)	0.0005
β_1	0.9
β_2	0.999
Activation function	LeakyReLU

SHM system

The Tongling Bridge, built in 2015, is a long-span highway-railway dual-purpose bridge. As shown in Figure 7(a), the entire bridge consists of the North Approach Bridge, the main span across the river, and the South Approach Bridge. The total length of the main span across the river is 1290 m, with spans arranged as 90 + 240 + 630 + 240 + 90 m. The main span is 630 m, allowing for bidirectional navigation in a single span, and the height of the bridge deck is 32 m. The main tower is a rhombic reinforced concrete structure with an inverted Y-shaped design above the bridge deck, and the tower height is 212 m. An advanced SHM system is applied to monitor the structural condition during its in-service period, ensuring its stability. The SHM system includes a large number of sensors installed on the bridge to measure acceleration, displacement, strain, structural temperature, air temperature, wind speed, humidity, and more. Acceleration, as a key sensor data for monitoring the vibration of the bridge under the influence of vehicle and environmental loads, is measured by 15 acceleration sensors installed on the bridge deck. The sampling frequency is 100 Hz, and the monitoring points are depicted in Figure 7(b).

Forecasting results

Figure 8 presents the predicted results of 14 acceleration sensors in the time domain. In this visualization, both the measured and predicted signals from all 14 sensors are concurrently displayed to highlight the predictive efficacy of PSA-CGAN. To enhance clarity regarding the prediction details, we opted for a signal with a sampling length of 5 s and a sampling frequency of 100 Hz.

The figure demonstrates PSA-CGAN's successful anticipation of signals, irrespective of whether they originate from vehicle-induced or environmental stimuli.
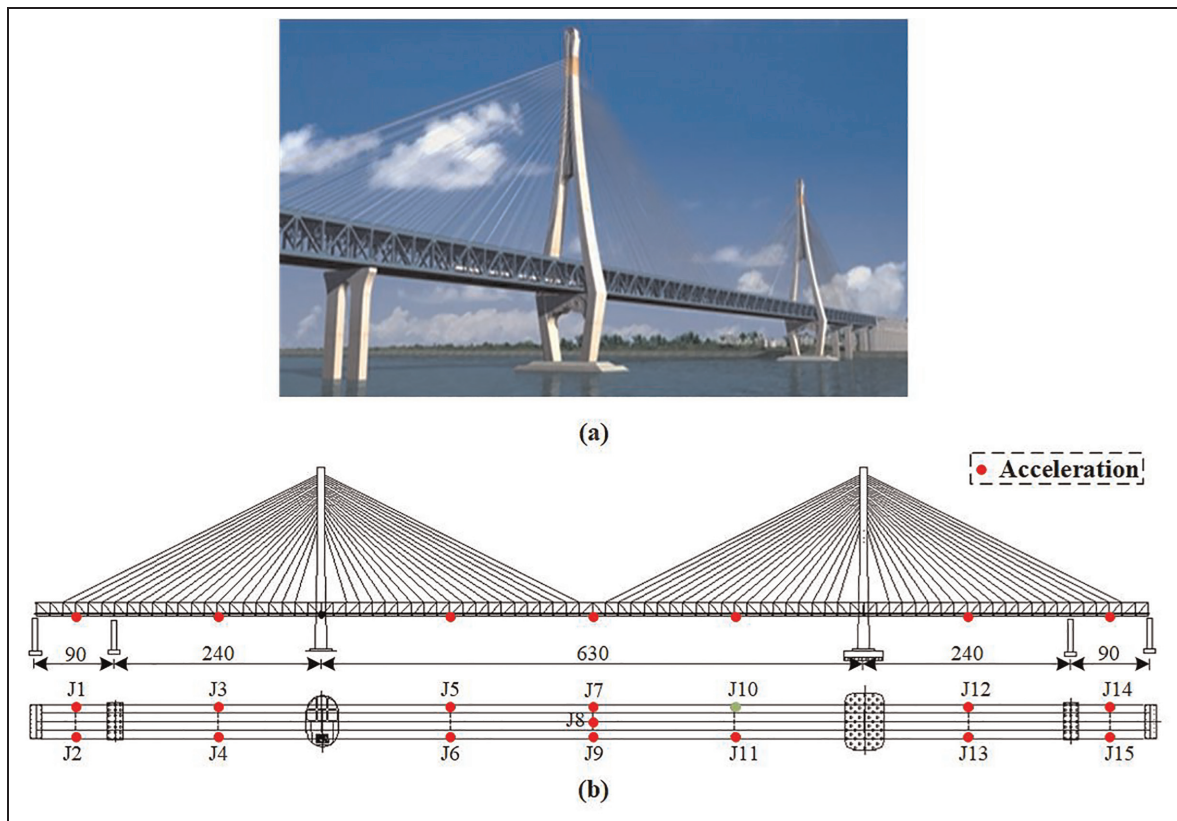
Figure 7. The schematic chart of the Tongling Bridge: (a) General view and (b) Front view.

Precise signal prediction and the identification of vehicle positions, potentially within safe zones, contribute significantly to structural safety assessments. The capability to remotely forecast future signals further fortifies confidence in structural safety. Additionally, predicting accelerometer responses from sensors ensures the ongoing collection of actual measurement results by the SHM system, ensuring data integrity.

Three distinct remote prediction intervals are selected to underscore the method's excellence: 10, 30, and 60 s. The comparative results of their predicted signals against measured signals are depicted in Figures 8 to 10. Evidently, the PSA-CGAN method exhibits robust stability in remote predictions across varying intervals, maintaining consistent alignment between predicted and measured signals. Upon comparison, Figures 8 to 10 reveal that with increasing time intervals, there may be minor fluctuations in the stability of predicted data for some sensors, yet these fluctuations remain within a manageable range.

Figure 11 showcases the correlation between predicted and measured signals from 14 sensors at three different intervals (10, 30, and 60 s). The correlation plot reveals a well-distributed arrangement of data points on both sides of the positive correlation curve

($y = x$), vividly highlighting a robust linear correlation between predicted and measured signals. Moreover, as the time intervals increase, the number of scattered data points on the positive correlation curve grows, yet they consistently adhere closely to the curve. This underscores the outstanding generalization capability of the proposed PSA-CGAN, ensuring reliable predictive outcomes across diverse sensor signals and various signal scenarios.

Application case study II: Z24 bridge

SHM system

Z24 Bridge spans between Bern and Zurich in Switzerland and is a post-tensioned concrete box girder bridge. Figure 12 provides an overview mapping of Z24 Bridge. The main span of the bridge is 30 m, with side spans of 14 m on each side, resulting in a total length of 60 m and a width of 8.6 m. Constructed in 1963, the bridge was in use for 35 years and was dismantled at the end of 1998. To address the gap in the study of the actual damage process of the bridge, a comprehensive SHM study was conducted on Z24 Bridge from November 1997 to September 1998, just
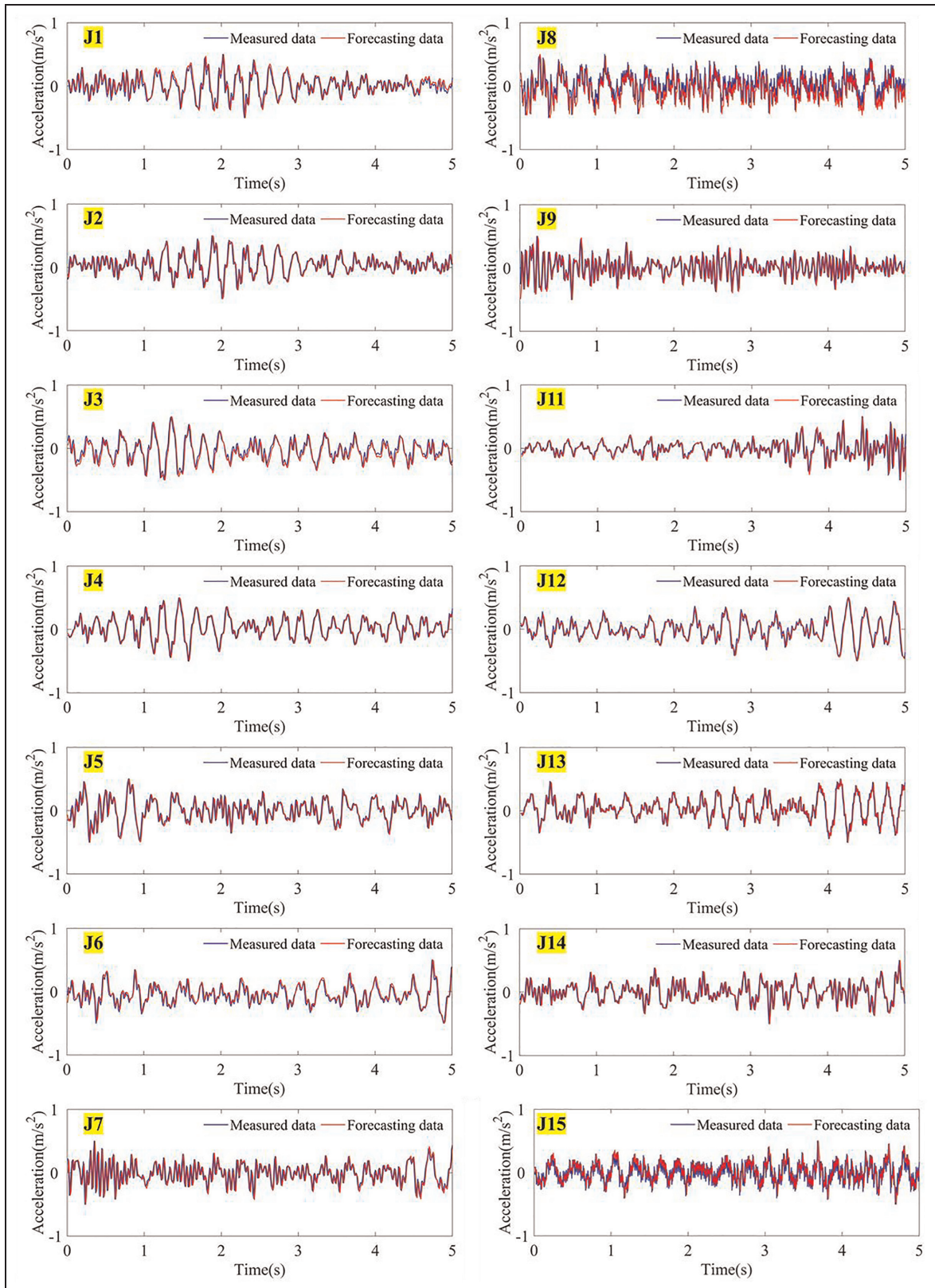
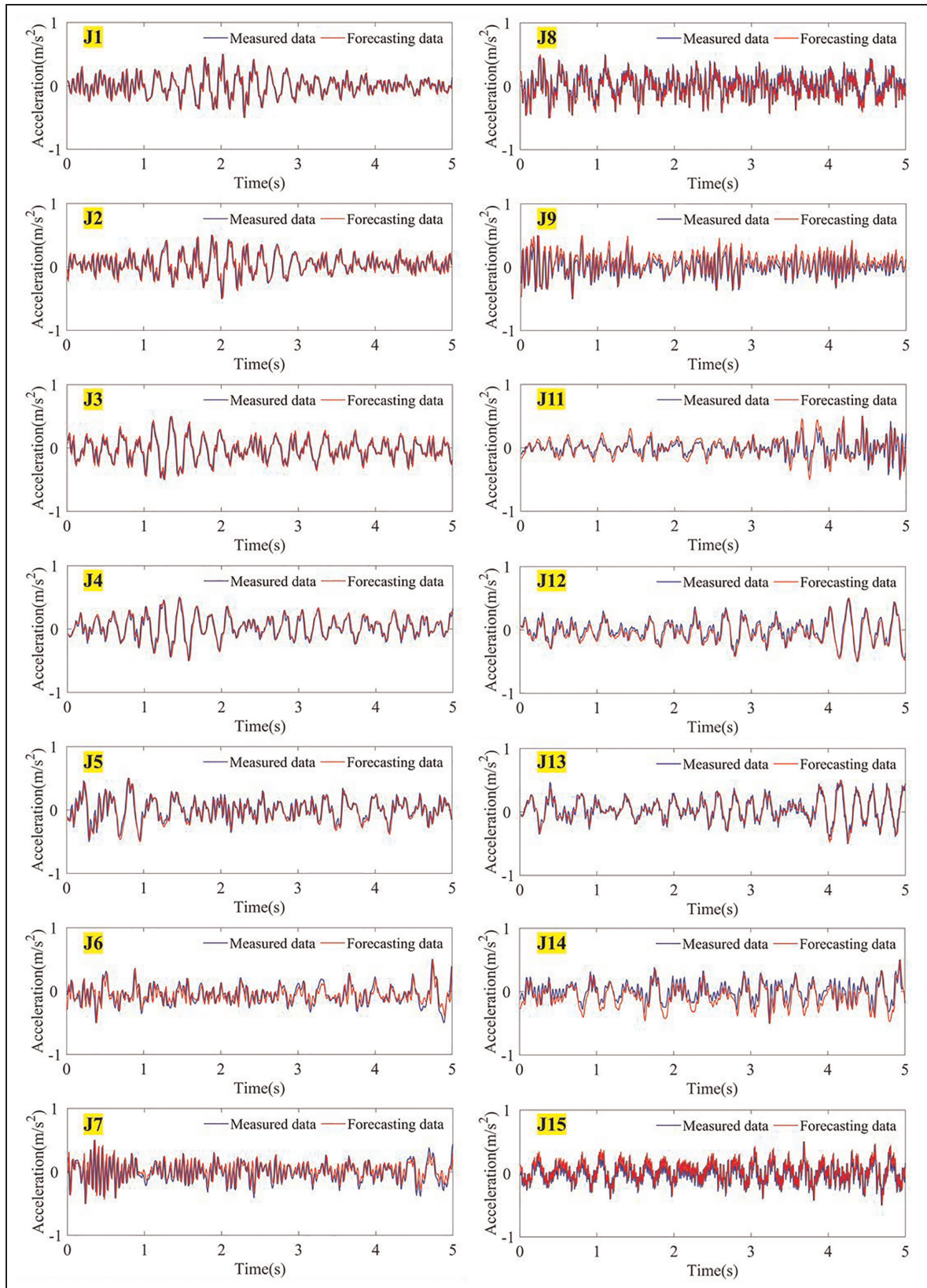**Figure 8.** Measured and forecasting data results for 10-s far-forecasting intervals.

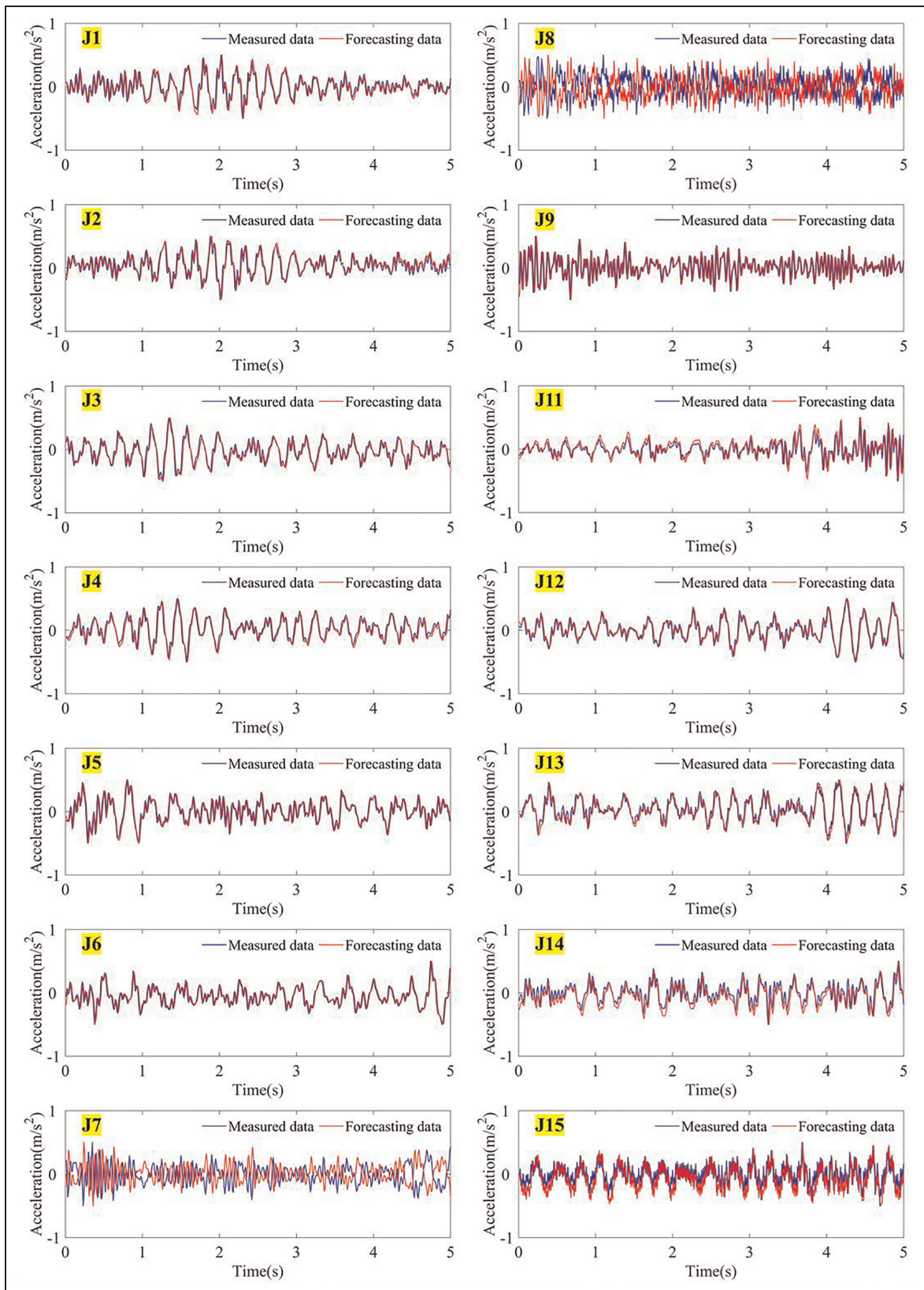**Figure 9.** Measured and forecasting data results for 30-s far-forecasting intervals.

Figure 10. Measured and forecasting data results for 60-s far-forecasting intervals.
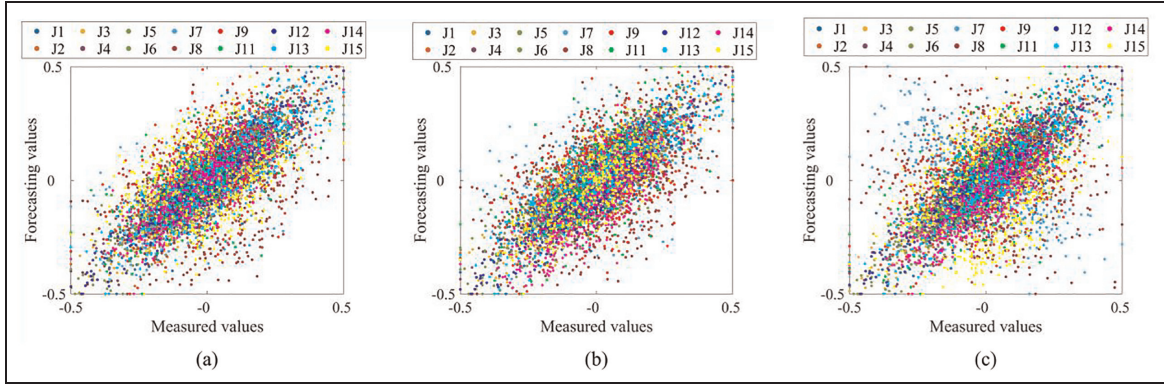
Figure 11. Correlation between measured data and forecasted data at different intervals: (a) 10-s, (b) 30-s, and (c) 60-s.
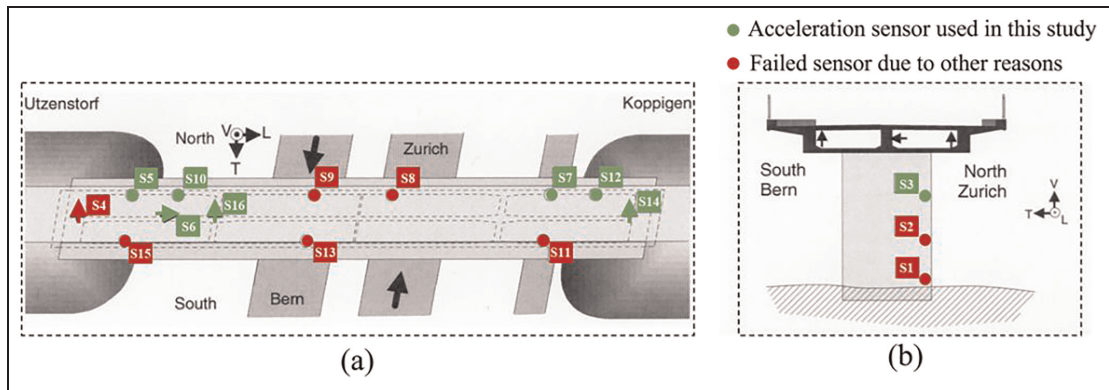

Figure 12. The schematic chart of the Z24 bridge: (a) Vertical view and (b) End view.

Table 2. Progressive damage period implemented on the Z24 bridge.

Damage number	Time	Description
PD0	23/02/1998	No Damage, Pier Hinge Added (Baseline)
PD1	10/08/1998	Settlement of pier, 20 mm
PD2	12/08/1998	Settlement of pier, 40 mm
PD3	17/08/1998	Settlement of pier, 80 mm
PD4	18/08/1998	Settlement of pier, 95 mm
PD5	19/08/1998	Tilt of foundation
PD6	20/08/1998	No Damage, Pier Restored
PD7	25/08/1998	Spalling of concrete, 12 m^2
PD8	26/08/1998	Spalling of concrete, 24 m^2
PD9	27/08/1998	Simulation of landslide
PD10	31/08/1998	Formation of concrete hinges
PD11	02/09/1998	Failure of anchor heads
PD12	03/09/1998	Failure of anchor heads #2
PD13	07/09/1998	Rupture of tendons #1
PD14	08/09/1998	Rupture of tendons #2
PD15	09/09/1998	Rupture of tendons #3

before its demolition. A modern SHM system was employed for quantitative assessment of the structural condition. The design of the SHM system took into account the importance of the monitoring object and vulnerability analysis of monitoring locations. Vibration is a crucial aspect of the bridge monitoring, significantly impacting the safety and overall health of the structure. Therefore, monitoring the acceleration of the bridge became a fundamental and intuitive parameter for assessing vibration response. In Figure 12, the arrangement diagram of the SHM system for the bridge consists of 15 acceleration sensors. Red dots indicate sensors that failed due to reasons other than damage, while green dots represent the acceleration sensors used in this study. These sensors captured vibration responses induced by both vehicle loads and environmental loads, with a sampling frequency of 100 Hz.

Data preparation and evaluation metrics

To investigate the impact of structural damage on the bridge, a comprehensive series of 14 progressive damage experiments was conducted between November 1997 and September 1998, with the specific damage

processes outlined in Table 2. Various sensors were strategically placed on the bridge to measure acceleration, temperature, humidity, rainfall, wind speed, and wind direction. Each hour, accelerometers recorded the bridge's vibrations at a frequency of 100 Hz for approximately 10 min, resulting in each sample containing a total of 65,536 acceleration values.

Acceleration is a paramount parameter in identifying structural damage to the bridge. This study utilized the dataset from sensors S3, S5, S6, S7, S10, S12, S14, and S16, with their locations depicted in Figure 12. Predictions were made at 5-s intervals, spanning 5-s data, 30-s intervals, and 60-s intervals, aiming to assess the predictive efficacy of the PSA-CGAN method.

To comprehensively evaluate the predictive performance of the forecasting model, this study employs three key evaluation metrics: Normalized Root Mean Square Error (NRMSE), Mean Absolute Percentage Error (MAPE), and Mean Absolute Error (MAE). NRMSE serves as a relative measure of performance, allowing for the convenient assessment of prediction error magnitude through relative comparisons of the same samples. MAPE is commonly used to illustrate the percentage of errors between measured values and target values. MAE represents the average deviation level between measured values and target values. Smaller values for these metrics indicate superior performance, with values closer to zero considered indicative of better evaluation performance. To address the issue of the denominator approaching zero in the MAPE calculation, this article implements a modified version of the MAPE formula that includes a small threshold value ε. The modified formula is as follows:

$$\text{NRMSE} = \sqrt{\frac{1}{n}\sum_{i=1}^{n}\left|\frac{y_i - y_i'|^2}{y_{\max} - y_{\min}}\right|} \tag{9}$$

$$\text{MAPE}_{\text{modified}} = \frac{100}{n}\sum_{i=1}^{n}\left|\frac{y_i - y_i'}{\max(|y_i|, \varepsilon)}\right| \tag{10}$$

$$\text{MAE} = \frac{1}{n}\sum_{i=1}^{n}|y_i - y_i'| \tag{11}$$

where y_i denote measured data, y_i' denote forecasting data, and n is the number of data, $\varepsilon = 0.001$.

Training and testing

In the proposed PSA-CGAN model, progressive growing and self-attention mechanisms are employed to accurately capture signal characteristics in measurement series, effectively reducing nonlinear and nonstationary variations, thereby enhancing the predictability

of time series. Predictive results for different interval lengths (10, 30, 60 s) under PD6 damage conditions are illustrated in Figures 13 to 15. Clearly, the method consistently demonstrates excellent predictive performance across these scenarios, successfully forecasting data from diverse sensors and affirming its precision and generalization. Notably, it's observed that the model's accuracy experiences only marginal variations with increasing interval lengths.

As the prediction interval increases, some sensors, such as S14, exhibit poorer results due to the extended interval, which negatively impacts prediction accuracy. Additionally, the sensor arrangement in the SHM system leads to distinct data characteristics for different sensors. Feature analysis indicates that significant changes in time series features influence the prediction results. Each sensor operates in a constantly changing environment, and these environmental variations contribute to differences in prediction outcomes. Overall, the predictive performance of PSA-CGAN remains robust and effective.

Data correlation is a crucial metric for assessing the accuracy of predictions. Figure 16 illustrates a robust correlation between the predicted and measured values of eight sensors at three distinct intervals. As the time interval expands, the correlation gradually diminishes. This underscores the influence of time interval length on the precision of data predictions.

Data forecasting in diverse long-term series

Additionally, the predictions for the data of diverse long-term series from eight sensors under PD6 damage conditions (5, 10, 20 s) are conducted. NRMSE, MAPE, and MAE were selected as one of the evaluation metrics for the PSA-CGAN method to assess the predictive efficacy of varied long-term series data (5, 10, 20 s). As depicted in Figure 17, three performance metrics for all eight sensors are consistently low across the three different prediction data lengths. This implies that PSA-CGAN exhibits robust predictive capabilities across varying data lengths and sensors. Furthermore, the stability of the method is evident, as three performance metrics remain steady with an increase in data length. Although a slight downward trend suggests a marginal reduction in predictive data capabilities, overall, the method demonstrates resilience and effective predictive performance.

Data forecasting in progressive damage period

Modal identification is pivotal for monitoring structural conditions and detecting damage. However, accurate and timely prediction of damage data are critical
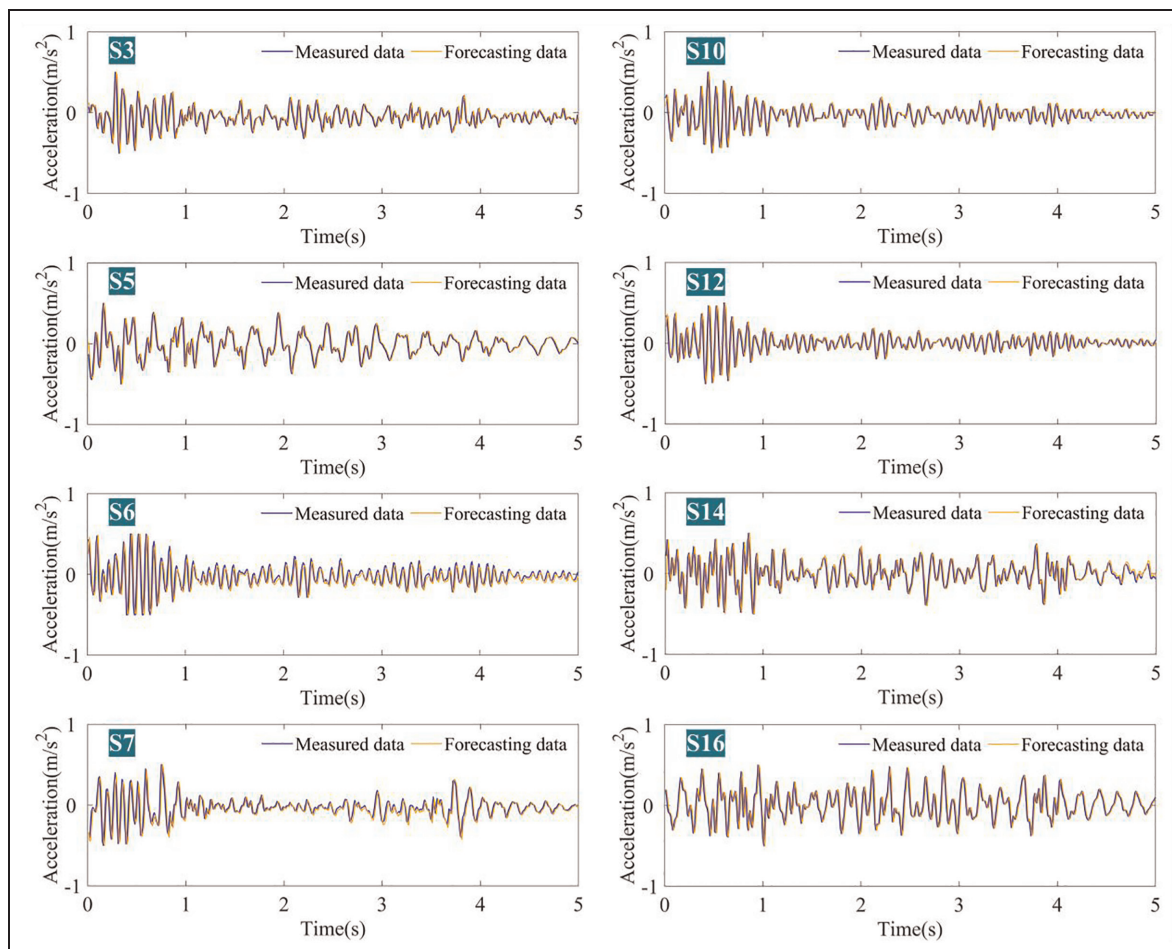
Figure 13. Measured and forecasting data results for 10-s far-forecasting intervals.

across diverse operational scenarios, emphasizing the significance of precise and stable data prediction methods. To showcase the superiority of the proposed PSA-CGAN prediction method under various conditions, modal identification was employed to predict damage scenarios for the Z24 bridge.

Given the substantial volume and noise in data collected by SHM systems, utilizing parameter identification techniques like the random subspace identification algorithm becomes challenging when applying time-domain and frequency-domain techniques to bridge data. Frequency-domain decomposition (FDD) stands out as a method capable of directly and accurately identifying modal parameters. In this study, FDD was applied for modal identification on measured and predicted data for 16 operational scenarios. FDD breaks down signals into sine components of varying frequencies and amplitudes, extracting latent dynamic information. Modal parameter identification involved a

comparison of measurement and prediction results from eight sensors, assessing the robustness and accuracy of the proposed method, as depicted in Figures 18 and 19.

These results underscore the high-quality data prediction capabilities of PSA-CGAN. Figure 18(a) illustrates the natural frequencies of the first six modes for measured and predicted data under 16 progressive damage scenarios. Figure 18(b) details the errors in these modal natural frequencies. Likewise, Figure 19(a) showcases the damping ratios of the first six modes for measured and predicted data under 16 progressive damage scenarios, and Figure 19(b) presents the errors in these damping ratios. These figures reveal that prediction errors for natural frequencies are within 0.5 Hz, and errors for signal-to-noise ratios are within 0.025%, confirming the high accuracy of the predicted results. Overall, the predicted data effectively identified modal parameters for six modes, affirming the outstanding
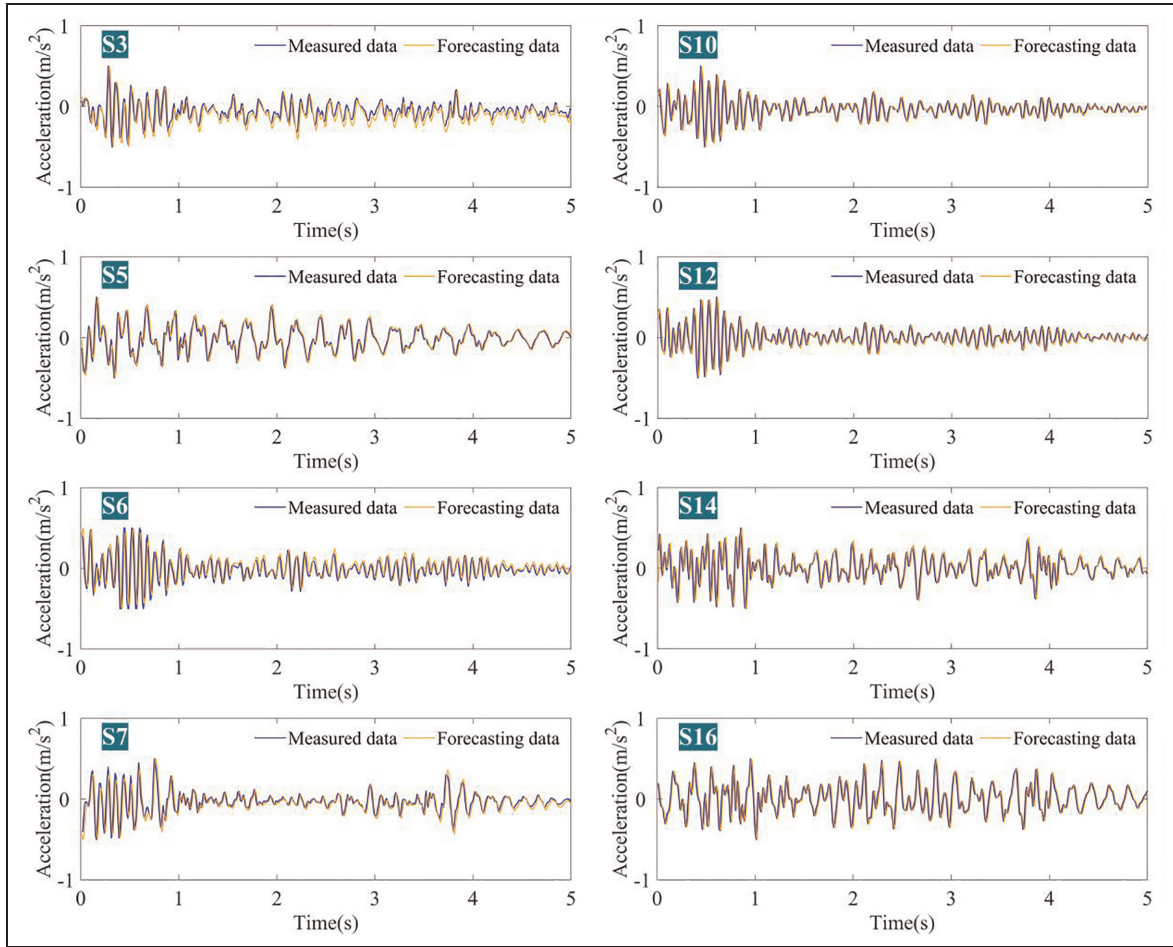
Figure 14. Measured and forecasting data results for 30-s far-forecasting intervals.

capability of the PSA-CGAN model in structural damage prediction.

Discussion on the case study

To fully comprehend the impact of progressive growing architecture and self-attention mechanisms on the PSA-CGAN model, this study provides a detailed analysis through comparative experiments. Three models were utilized for comparison: the PSA-CGAN model with self-attention and progressive growing (PSA-CGAN), the PSA-CGAN model without self-attention (PSA-CGAN-N-SA), and the PSA-CGAN model without progressive growing (PSA-CGAN-N-PG). The comparative experiments were conducted across three different context-free time intervals (100 data points, 1000 data points, and 2000 data points). All algorithms were executed on computers with identical configurations, as detailed in section "Application case study I: Tongling bridge."

The results of the comparison are presented in Table 3. It was observed that in various context-free

prediction scenarios, the PSA-CGAN model outperformed the models lacking progressive growing and self-attention mechanisms. This demonstrates that the PSA-CGAN model effectively captures both long-term and short-term features in time series through the integration of progressive growing and self-attention mechanisms, thereby significantly enhancing the efficiency and accuracy of the prediction methods.

To gain a thorough understanding of the predictive prowess of the PSA-CGAN model, PSA-CGAN alongside several prominent forecasting models (including Probabilistic Forecasting with Autoregressive Recurrent Networks (DeepAR), Gated Recurrent Unit (GRU), and Long Short-Term Memory (LSTM)) are employed to predict context-free scenario data across 16 diverse operational conditions. Various context-free time intervals were explored, and a comparative analysis ensued. All algorithms were executed on a computer with the same configuration as detailed in section "Application case study I: Tongling bridge."

Figure 20 delineates the predictive performance analysis of PSA-CGAN and the three other
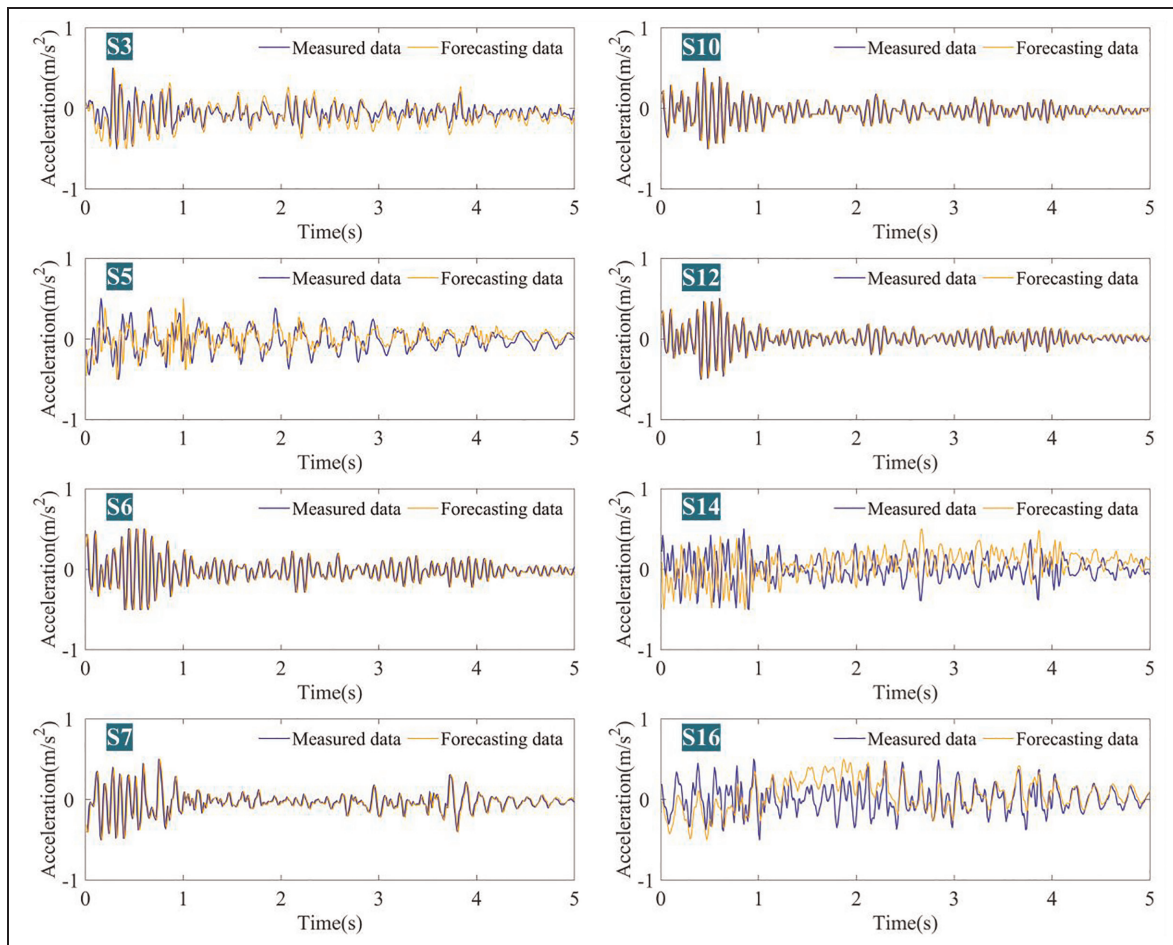
Figure 15. Measured and forecasting data results for 60-s far-forecasting intervals.

Table 3. Comparative experiments of the main component in PSA-CGAN.

Model	500 data points			1000 data points			2000 data points		
	NRMSE	MAPE	MAE	NRMSE	MAPE	MAE	NRMSE	MAPE	MAE
PSA-CGAN	**0.0021**	**1.4794**	**0.0855**	**0.0135**	**2.8902**	**0.0942**	**0.0223**	**4.9321**	**0.1102**
PSA-CGAN-N-SA	0.023	5.56	0.3612	0.043	8.35	0.4235	0.052	12.56	0.5631
PSA-CGAN-N-PG	0.012	3.86	0.2811	0.021	7.54	0.3954	0.031	9.05	0.4269

PSA-CGAN: convolutional generative adversarial network with progressive growing and self-attention; PSA-CGAN-N-SA: PSA-CGAN model without self-attention; PSA-CGAN-N-PG: PSA-CGAN model without progressive growing.
Bold part represents the optimal score.

interpolation models under the PD6 operational condition. The PSA-CGAN model consistently exhibits high precision and stable predictive capabilities in context-free scenarios. This is chiefly attributed to the inherent support for progressive growth and self-attention mechanisms within the PSA-CGAN framework, enabling the extraction of pivotal long- and short-term information from context-free sensors. Specifically, as depicted in Table 4, across the 16 scenarios, the PSA-CGAN model showcases superior predictive performance and heightened accuracy, generally yielding the smallest values for NRMSE, MAPE, and MAE. In scenarios with contextual information, DeepAR displays robust predictive abilities, yet its effectiveness diminishes in context-free scenarios. Furthermore, while GRU and LSTM stand as typical forecasting
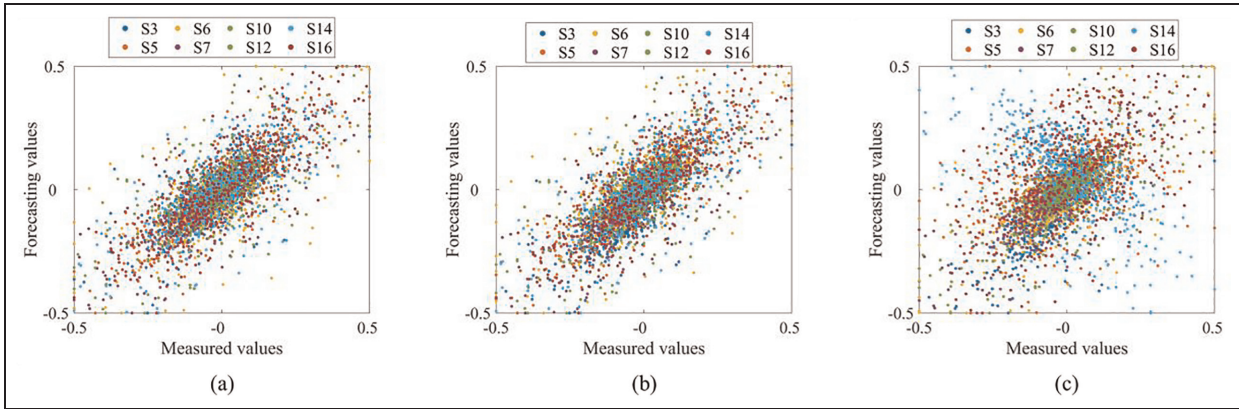
Figure 16. Correlation between measured data and forecasted data at different intervals; (a) 10-s, (b) 30-s, and (c) 60-s.
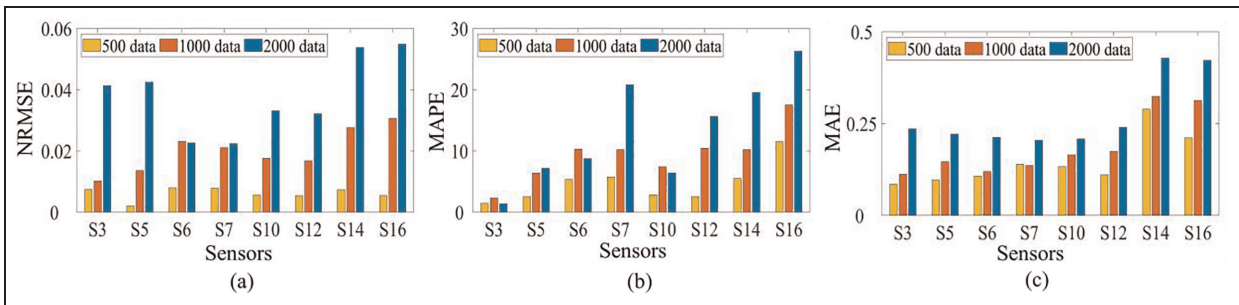

Figure 17. The performance metrics of Z24 bridge in different forecasting lengths (a) NRMSE, (b) MAPE, and (c) MAE.
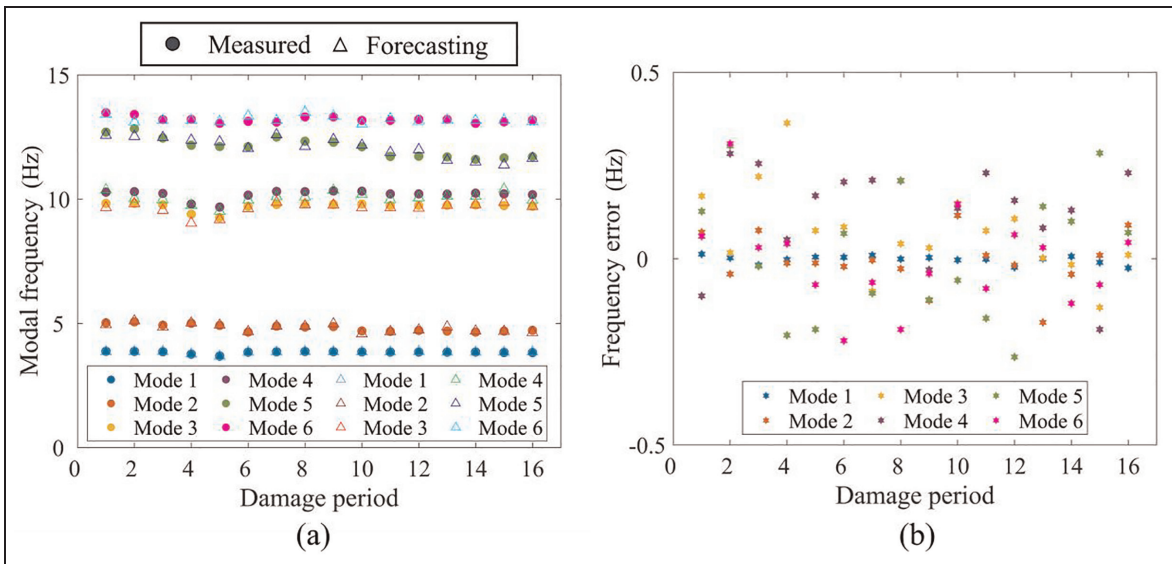

Figure 18. Comparison of natural frequency in different damage scenarios: (a) Measured and forecasting natural frequency and (b) Measured and forecasting natural frequency error.
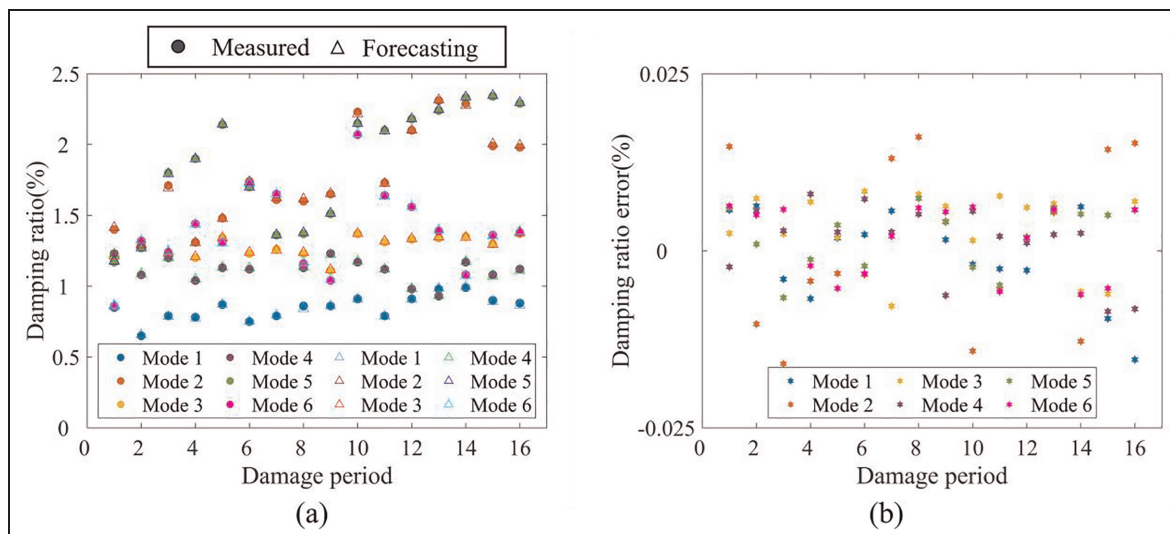
Figure 19. Comparison of damping ratio in different damage scenarios: (a) Measured and forecasting damping ratio and (b) Measured and forecasting damping ratio error.
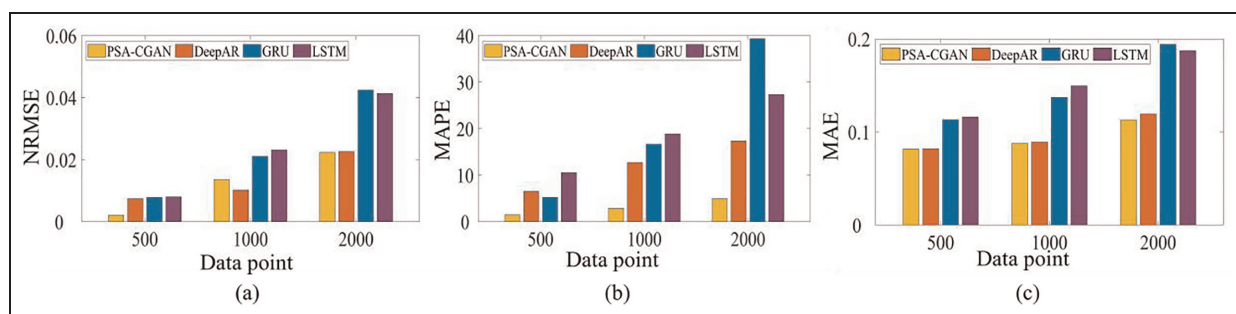

Figure 20. Comparison of different models: (a) NRMSE, (b) MAPE, and (c) MAE.

methods in recurrent neural networks, they demonstrate commendable performance in certain scenarios but exhibit lower accuracy in context-free situations. In summary, the PSA-CGAN model demonstrates robust predictive capabilities, high accuracy, and remarkable generalization, rendering it well-suited for deployment across diverse sensor arrays.

Conclusion

This article proposes a PSA-CGAN mechanisms for predicting context-free data. The method applies GANs to tasks involving long-time series. Additionally, the article incorporates two crucial mechanisms—progressive growth and self-attention—to capture long- and short-term features in time series, significantly enhancing the efficiency and accuracy of the prediction method. Moreover, the method is applied to two different bridge cases, the Tongling

public-rail dual-use bridge and the Z24 bridge, to validate its versatility and real-time prediction capability. Specifically, two cases are used: predicting acceleration data (undamaged) for the Tongling public-rail bridge and predicting acceleration data (damaged) for the benchmark Z4 model. Furthermore, the implemented PSA-CGAN independently trains each sensor to predict long acceleration series obtained during different operating conditions of the SHM system. The main conclusions of this study are as follows:

1. The method is adaptable to both single and multiple sensors, demonstrating wide applicability. Even in SHM systems with a limited number of sensors, it can quickly and effectively make predictions.
2. Based on the results from the two bridges, the method shows good predictive performance in both damaged and undamaged scenarios, indicating broad applicability.

Table 4. Comparison of forecasting performances under different damage scenarios.

Damage type	Metric	PSA-CGAN	DeepAR	GRU	LSTM
PD0	NRMSE	0.0175	0.0234	**0.0173**	0.0517
	MAPE	1.4382	2.3242	**1.3771**	5.3245
	MAE	**0.0131**	0.0443	0.0252	0.5611
PD1	NRMSE	**0.0041**	0.045	0.0264	0.0316
	MAPE	**2.5512**	6.4012	7.1624	11.7959
	MAE	**0.0254**	0.0735	0.1142	0.2935
PD2	NRMSE	**0.0178**	0.0451	0.0534	0.0824
	MAPE	**5.3452**	10.323	8.7544	11.2321
	MAE	**0.0436**	0.0981	0.1108	0.1198
PD3	NRMSE	**0.0569**	0.0897	0.1523	0.1123
	MAPE	**5.7512**	10.2115	20.8121	23.2121
	MAE	**0.0595**	0.1007	01221	0.1327
PD4	NRMSE	0.0546	0.0526	**0.0456**	0.0754
	MAPE	**8.4562**	16.4567	17.7895	25.8412
	MAE	**0.0725**	0.2156	0.2475	0.3044
PD5	NRMSE	**0.0541**	0.1312	0.2542	0.1521
	MAPE	**5.2124**	11.5421	15.2102	15.5122
	MAE	**0.0124**	0.2456	0.3457	0.3471
PD6	NRMSE	**0.0245**	0.0741	0.0785	0.0801
	MAPE	**2.8112**	7.4123	6.412	13.5123
	MAE	**0.0302**	0.0617	0.0603	0.1093
PD7	NRMSE	**0.1512**	0.1971	0.3654	0.4512
	MAPE	**5.5123**	7.8453	15.5423	15.6541
	MAE	**0.0172**	0.1536	0.2356	0.2453
PD8	NRMSE	**0.1642**	0.1842	0.3875	0.2631
	MAPE	**5.8542**	10.6452	17.3423	23.621
	MAE	**0.0022**	0.1874	0.2542	0.2743
PD9	NRMSE	**0.0235**	0.0751	0.0852	0.0954
	MAPE	**2.5531**	10.4521	15.6421	16.3459
	MAE	**0.0545**	0.1712	0.2623	0.2698
PD10	NRMSE	**0.0426**	0.0845	0.1346	0.0845
	MAPE	**4.5232**	19.2454	19.8423	21.2751
	MAE	**0.0754**	0.1742	0.2151	0.2745
PD11	NRMSE	**0.0421**	0.0564	0.1512	0.1903
	MAPE	**5.5341**	10.2125	19.561	20.5431
	MAE	**0.0742**	0.1512	0.1835	0.1956
PD12	NRMSE	**0.0541**	0.5413	0.7415	0.1512
	MAPE	**9.5637**	22.5123	24.5124	20.8416
	MAE	**0.0931**	0.1535	0.2489	0.1533
PD13	NRMSE	**0.0512**	0.245	0.2987	0.3512
	MAPE	**11.5122**	17.5331	26.2753	21.5664
	MAE	**0.1223**	0.1653	0.2765	0.2136
PD14	NRMSE	**0.0564**	0.1623	0.3642	0.4562
	MAPE	**5.5123**	7.1874	15.5453	17.8158
	MAE	**0.0552**	0.0923	0.1256	0.2453
PD15	NRMSE	**0.0542**	0.1612	0.3530	0.3951
	MAPE	**2.5122**	3.5312	16.5621	25.5631
	MAE	**0.0634**	0.0736	0.2364	0.3654

PSA-CGAN: convolutional generative adversarial network with progressive growing and self-attention; PSA-CGAN-N-SA: PSA-CGAN model without self-attention; PSA-CGAN-N-PG: PSA-CGAN model without progressive growing.
Bold part represents the optimal score.

3. In long-time series predictions, PSA-CGAN performs well at different distance intervals. However, as the interval distance increases, its accuracy decreases.

4. PSA-CGAN, utilizing convolutional neural network architecture, self-attention, and progressive growth mechanisms, extends its applicability to long-time series prediction. It allows modeling

remote dependencies from convolutional feature mappings. While performing well for the majority of time series prediction tasks, it exhibits poor predictive capabilities for long-time series of certain sensors (S14, S16).

5. Comparing this method with current advanced prediction methods using three different evaluation criteria (NRMSE, MAPE, MAE), it is evident that, in 16 comparative scenarios, this method's evaluation values are closer to 0, indicating better predictive accuracy.

Overall, the results suggest that the PSA-CGAN mechanisms is a promising and practical solution for predicting context-free data. It serves as an effective and fast damage prediction tool.

Declaration of conflicting interests

Funding

ORCID iDs

Zhenwei Zhou https://orcid.org/0000-0002-1940-2697
Chunfeng Wan https://orcid.org/0000-0002-4236-6428
Liyu Xie https://orcid.org/0000-0001-5777-0645

References

1. Cross EJ, Koo KY, Brownjohn JMW, et al. Long-term monitoring and data analysis of the Tamar Bridge. *Mech Syst Signal Process* 2013; 35(1–2): 16–34.
2. Whelan MJ and Janoyan KD. Design of a robust, high-rate wireless sensor network for static and dynamic structural monitoring. *J Intell Mater Syst Struct* 2009; 20(7): 849–863.
3. Kim S, Pakzad S, Culler D, et al. Health monitoring of civil infrastructures using wireless sensor networks. In: *IPSN 2007 6th International symposium on information processing in sensor networks*, Cambridge, MA, USA, 2007, pp. 254–263.
4. Ko JM and Ni YQ. Technology developments in structural health monitoring of large-scale bridges. *Eng Struct* 2005; 27(12): 1715–1725.
5. Magalhães F, Cunha A and Caetano E. Vibration based structural health monitoring of an arch bridge: from automated OMA to damage detection. *Mech Syst Signal Process* 2012; 28: 212–228.
6. Beskhyroun S, Wegner LD and Sparling BF. Integral resonant control scheme for cancelling human-induced vibrations in light-weight pedestrian structures. *Struct Control Health Monit* 2011; 19(1): 55–69.
7. Chapuis B. *Introduction to structural health monitoring*. Springer, 2018. pp. 1–11.
8. Fassois SD and Kopsaftopoulos FP. Statistical time series methods for vibration based structural health monitoring. New trends in strcutural health monitoring, Vienna, Austria, vol. 542, 2013, pp. 209–264.
9. Han Q, Ma Q, Xu J, et al. Structural health monitoring research under varying temperature condition: a review. *J Civ Struct Health Monit* 2021; 11(1): 149–173.
10. Kang F, Li J and Dai J. Prediction of long-term temperature effect in structural health monitoring of concrete dams using support vector machines with Jaya optimizer and salp swarm algorithms. *Adv Eng Softw* 2019; 131: 60–76.
11. Wan H-P and Ni Y-Q. Bayesian multi-task learning methodology for reconstruction of structural health monitoring data. *Struct Health Monit* 2019; 18(4): 1282–1309.
12. Wan H-P and Ni Y-Q. Bayesian modeling approach for forecast of structural stress response using structural health monitoring data. *J Struct Eng* 2018; 144(9): 1–12.
13. Wang YW and Ni YQ. Bayesian dynamic forecasting of structural strain response using structural health monitoring data. *Struct Control Health Monit* 2020; 27(8). DOI: 10.1002/stc.2575
14. Wang QA, Wang CB, Ma ZG, et al. Bayesian dynamic linear model framework for structural health monitoring data forecasting and missing data imputation during typhoon events. *Struct Health Monit* 2022; 21(6): 2933–2950.
15. Ren P, Chen X, Sun L, et al. Incremental Bayesian matrix/tensor learning for structural monitoring data imputation and response forecasting. *Mech Syst Signal Process* 2021; 158: 107734.
16. Green DKE and Jaspan A. Applied Bayesian structural health monitoring: inclinometer data anomaly detection and forecasting. *Proc Appl Math Mech*. Epub ahead of print 10 December 2023. DOI: 10.1002/pamm. 202300132.
17. Yi L, Ding Y, Hou J, et al. Structural health monitoring data cleaning based on Bayesian robust tensor learning. *Struct Health Monit* 2022; 22(4): 2169–2192.
18. Lai L, Dong Y and Smyl D. SHM-informed life-cycle intelligent maintenance of fatigue-sensitive detail using Bayesian forecasting and Markov decision process. *Struct Health Monit*. Epub ahead of print 12 April 2023. DOI: 10.1177/14759217231160412.
19. Wei B, Yuan D, Li H, et al. Combination forecast model for concrete dam displacement considering residual correction. *Struct Health Monit* 2019; 18(1): 232–244.
20. Yang N and Bai X. Forecasting structural strains from long-term monitoring data of a traditional Tibetan building. *Struct Control Health Monit* 2019; 26(1): e2300.
21. Qu B, Liao P and Huang Y. Outlier detection and forecasting for bridge health monitoring based on time series

intervention analysis. *Struct Durab Health Monit* 2022; 16(4): 323–341.

22. Zhang P, Ren P, Liu Y, et al. Autoregressive matrix factorization for imputation and forecasting of spatiotemporal structural monitoring time series. *Mech Syst Signal Process* 2022; 169: 108718.

23. Wang C and Zhang P. A combined method of autoregressive model and matrix factorization for recovery and forecasting of cyclic structural health monitoring data. *Mech Syst Signal Process* 2023; 202: 110703.

24. Wang Q-A, Zhang C, Ma Z-G, et al. Modelling and forecasting of SHM strain measurement for a large-scale suspension bridge during typhoon events using variational heteroscedastic Gaussian process. *Eng Struct* 2022; 251: 113554.

25. Goodfellow I, Pouget-Abadie J, Mirza M, et al. Generative adversarial networks. *Commun ACM* 2014; 63(11): 139–144.

26. Gui J, Sun Z, Wen Y, et al. A review on generative adversarial networks: algorithms, theory, and applications. *IEEE Trans Knowl Data Eng* 2021; 14(8): 1–1.

27. Pan Z, Yu W, Yi X, et al. Recent progress on generative adversarial networks (GANs): a survey. *IEEE Access* 2019; 7: 36322–36333.

28. Yoon J, Jordon J and Van Der Schaar M. GAIN: Missing data imputation using generative adversarial nets. In: *35th International Conference of Machine Learning Stockholm, Sweden, ICML 2018*, vol. 13, pp. 9042–9051, 2018.

29. Gao S, Zhao W, Wan C, et al. Missing data imputation framework for bridge structural health monitoring based on slim generative adversarial networks. *Meas J Int Meas Confed* 2022; 204: 112095.

30. Hou J, Jian H, Wan C, et al. Deep learning and data augmentation based data imputation for structural health monitoring system in multi-sensor damaged state. *Meas J Int Meas Confed* 2022; 196: 111206.

31. Gao S, Wan C, Zhou Z, et al. Enhanced data imputation framework for bridge health monitoring using Wasserstein generative adversarial networks with gradient penalty. *Structures* 2023; 57: 105277.

32. Jiang H, Wan C, Yang K, et al. Continuous missing data imputation with incomplete dataset by generative adversarial networks–based unsupervised learning for long-term bridge health monitoring. *Struct Health Monit*. Epub ahead of print 4 April 2021. DOI:.

33. Lei X, Sun L and Xia Y. Lost data reconstruction for structural health monitoring using deep convolutional generative adversarial networks. *Struct Health Monit* 2021; 20(4): 2069–2087.

34. Fan G, Li J and Hao H. Dynamic response reconstruction for structural health monitoring using densely connected convolutional networks. *Struct Health Monit* 2021; 20(4): 1373–1391.

35. Fan G, He Z and Li J. Structural dynamic response reconstruction using self-attention enhanced generative adversarial networks. *Eng Struct* 2023; 276: 115334.